Supplementary online material (SOM)

Investigating the effect of diagenesis on ESR dating of Middle Stone Age tooth samples from the open-air site of Lovedale, Free State, South Africa

Maïlys Richard[a,b,c,d], Edwige Pons-Branchu[b], Raanan Carmieli[e], Ifat Kaplan-Ashiri[e], Ana Alvaro Gallo[a], Giulia Ricci[f], Luisa Caneve[g], Kristen Wroth[h], Arnaud Dapoigny[b], Chantal Tribolo[i], Elisabetta Boaretto[j], Michael B. Toffolo[i]

[a] Centro Nacional de Investigación sobre la Evolución Humana (CENIEH), 09002 Burgos, Spain

[b] Laboratoire des Sciences du Climat et de l'Environnement (LSCE), GEOTRAC-LSCE/IPSL, UMR 8212, CEA-CNRS-UVSQ, Université Paris-Saclay, 91191 Gif-sur-Yvette, France

[c] Department of Early Prehistory and Quaternary Ecology, University of Tübingen, 72070 Tübingen, Germany

[d] Centre de Recherche Français à Jérusalem (CRFJ), USR 3132, 9100401, Jerusalem, Israel

[e] Department of Chemical Research Support, Weizmann Institute of Science, 7610001 Rehovot, Israel

[f] Department of Geosciences, University of Padova, 35131 Padova, Italy

[g]ENEA, 00044 Frascati, Italy

[h] Institut für Naturwissenschaftliche Archäologie, University of Tübingen, 72070 Tübingen, Germany

[i] Archéosciences Bordeaux, UMR 6034 CNRS-Université Bordeaux Montaigne, 33607 Pessac, France

[j] Scientific Archaeology Unit, Weizmann Institute of Science, 7610001 Rehovot, Israel

*Corresponding author: mailys.richard@cenieh.es

Materials and methods (supplementary text)

1. Sample collection and preparation

Dental tissues were mechanically separated and the enamel cleaned on both sides using a dentist drill. At least 20 µm were removed from the sides that were in contact with the dentine ('side 1') and the sediment ('side 2') to eliminate the volume irradiated by alpha particles. The enamel was ground and sieved using a 200 µm mesh sieve; the granulometric fraction ≤ 200 µm was used for the characterisation and dating analyses.

2. Micromorphology of sediments

The profile was cleaned back approximately 10 cm to expose a fresh section and micromorphology blocks were carefully carved out, consolidated with plaster bandages, and then left to fully dry. The blocks were then transported to PACEA-Transfert Sédimentologie et Matériaux at the University of Bordeaux (France) where they were impregnated with polyester resin under vacuum. The samples were then cut into slices, affixed to a glass slide, and polished to a thickness of ~30 µm. The slides were analysed using both a stereomicroscope and a petrographic microscope under both plane polarized light (PPL) and cross polarized light (XPL) at up to 400x magnification.

3. Electron spin resonance dating

The five fossil teeth were divided into several aliquots: one was kept intact to measure the natural ESR intensity and the others were irradiated at increasing doses. LOV1180 was split into five aliquots (9.7-9.9 mg) and irradiated using a ^{60}Co source at 40, 90, 240, and 610 Gy (Soreq Nuclear Research Center, Yavne, Israel). LOV1197 (5.1-5.9 mg), 1200 (9.3-10.1 mg), 1201 (10.2-11.0 mg), and 1205 (13.7-14.7 mg) were irradiated using a ^{137}Cs gamma source (CENIEH, Burgos, Spain) at 40, 64, 100, 250, 640, and 1600 Gy. For LOV1201 and 1205, for which more material was available, four additional aliquots were irradiated at 160, 400, 1000, and 2500 Gy.

LOV1180 was measured on an X-band spectrometer (ELEXSIS E-500, Bruker) at the Department of Chemical Research Support, Weizmann Institute of Science (Rehovot, Israel). Due to the small amount of available material (< 10 mg), enamel aliquots were loaded in small capillaries (internal ∅: 1 mm) to increase the height of each aliquot (~2 cm height). Each small

capillary was placed in a tube (internal ∅: 2 mm), which was used for the measurement of all aliquots and located at the same depth in the cavity for signal optimisation. Measurements were conducted at room temperature and repeated twice for each aliquot, using the following parameters: 10-20 scans, 1 mW microwave power, 1024 points resolution, 10 mT sweep width, 100 kHz modulation frequency, 0.1 mT modulation amplitude, 20.48 ms conversion time, and 5.12 ms time constant. It is generally advised to measure enamel aliquots at a microwave power ≤ 2 mW to avoid saturation (e.g., Grün, 1989). Dose response curves and equivalent doses (D_e) obtained for each series of measurements were then compared. For the other samples, LOV1197, 1200, 1201, and 1205, each aliquot was measured four times using an X-band spectrometer (Bruker EMXmicro-6/1) at the CENIEH and using the same parameters used for LOV1180. The equivalent doses were obtained by plotting the mean value of the ESR intensity calculated from the different series of measurements and associated standard deviations as a function of irradiation doses using Origin Pro 8 (Origin Lab Corporation, Northampton, USA). The dose response curves were obtained by extrapolation using a single saturation exponential (SSE) function (Yokoyama et al., 1985) and weighted by the inverse of the squared ESR intensity ($1/I^2$).

Regarding the dose rate, the gamma dose was measured *in situ* using a portable gamma-ray multichannel analyser connected to a NaI (Tl) probe Inspector 1000 (Canberra) in the section from the 1×1 square meter. The data were treated following the "threshold" technique (Mercier and Falguères, 2007). The beta dose rate was derived from the sediment sample collected with the teeth and measured by high-resolution low-background gamma-ray spectrometry equipped with a high-purity germanium detector (HPGe) at Bordeaux Montaigne University (Pessac, France). The cosmic dose rate was calculated taking into account the maximum sediment thickness above the sample (4.6 ± 1 m) according to Prescott and Hutton (1988).

4. Uranium-series dating

Uranium content (^{238}U) and isotopic ratios ($^{234}U/^{238}U$ and $^{230}Th/^{234}U$) were measured in enamel and dentine to model the U-uptake and to derive the dose rate according to Grün et al. (1988). The samples were dissolved in HNO_3 7M and spiked with a ^{229}Th-^{233}U-^{236}U solution calibrated against a Harwell Uraninite solution (HU-1), assumed to be at secular equilibrium. Separation and purification of U and Th isotopes follows Richard et al. (2015). Uranium and thorium

fractions were combined for measurements using a multi-collector inductively coupled plasma mass spectrometer (MC-ICP-MS) (Thermo Scientific™ Neptune Plus) fitted with a jet pump interface and a desolvating introduction system (aridus II) according to Pons-Branchu et al. (2014). ^{238}U, ^{235}U, ^{236}U, and ^{229}Th were measured on Faraday cups, ^{234}U and ^{230}Th on the ion counter (see details in Pons-Branchu et al., 2020).

5. Fourier transform infrared spectroscopy (FTIR)

FTIR measurements were carried out first on LOV1180 at the Kimmel Center for Archaeological Science (Weizmann Institute of Science) to assess the degree of crystallinity of enamel. One natural aliquot and one aliquot per irradiation dose (5 in total) were measured 3 times. Each aliquot (~0.1 mg) was mixed with KBr (~0.5 mg) and pressed into a 7-mm pellet. Analyses were performed using a Thermo Fisher Scientific Nicolet iS5 spectrometer in 32 scans at 4 cm^{-1} resolution in the 4000-400 cm^{-1} spectral range. After analysis, half of the pellet was discarded, whereas the remaining half was ground with more strength compared to the first analysis, and about 0.2 mg of KBr were added to press a new pellet for measurement. This procedure was repeated for a third measurement, applying more strength to the grinding. Spectra were analysed using OMNIC v. 9.6 and Macros Basic v. 8 and phase identification was based on standard literature (Farmer, 1974). The infrared splitting factor (IRSF) of the ν_4 absorption, which is the sum of the peaks at 604 and 567 cm^{-1} divided by the height of the valley between them (Weiner and Bar-Yosef, 1990), was plotted against the full width at half maximum (FWHM) of the ν_3 absorption at 1035 cm^{-1}, following the grinding curve method of Asscher et al. (2011a; 2011b) (Fig. 2). For LOV1197, 1200, 1201, and 1205, FTIR measurements were performed using a Thermo Fisher Scientific Nicolet 6700 spectrometer at the CENIEH. The same procedure and instrument settings were applied to obtain grinding curves. Two modern analogues, lamb ('LAM') and springbok ('SPR') teeth, were analysed to obtain reference spectra.

6. Raman micro-spectroscopy

Raman analyses were conducted at the CENIEH using a DXR Thermo Fisher Scientific Raman dispersive spectrometer, with a laser emitting at 532 nm. Enamel powder samples were placed on a glass slide on the stage of an Olympus microscope. The power radiation measured under the 50x microscope objective was about 1 mW. Acquisitions of 25 s and multiple additions were

used to improve the signal-to-noise ratio in the spectra. The spectrometer worked in a spectral range from 55 to 3350 cm^{-1}. The calibration of the spectrometer was done with a polystyrene standard (main band: 1000 cm^{-1}). For every sample, 10 different points were analysed. We focused our attention on the most intense peak of the spectra (961 cm^{-1}) corresponding to the symmetric stretching vibration of the PO_4^{3-} group. Peak location and FWHM were obtained by deconvoluting the spectra using the software OMNIC v. 8.2.

7. Scanning electron microscopy coupled with cathodoluminescence (SEM-CL)

SEM-CL was employed to study several enamel aliquots of LOV1180 that were exposed to increasing amounts of radiation (0, 40, 90, 240, and 610 Gy). The SEM-CL measurements were performed at the Department of Chemical Research Support (Weizmann Institute of Science) using a Gatan MonoCL4 Elite system installed on a Zeiss GeminiSEM 500 high-resolution SEM. The light was excited using an electron beam accelerated to 15 kV (with a 60 µm aperture); the collected light was directed to a monochromator with a spectral range of 200–1100 nm. The data was collected in Spectrum Imaging (SI) mode, where simultaneous SEM image and spectra were collected for a defined region of interest (ROI); that way both the spectral information and electron image could be correlated. SEM images were collected using the SE2 detector and CL was acquired with the 150 lines/mm grating centred on 550 nm and 1 mm entrance slit. Each spectrum image is composed of 420 pixels with a pixel size of 13 µm or 3.3 µm. The exposure time was set to 2 s per pixel.

8. Laser induced fluorescence (LIF)

LIF analyses were performed at the ENEA Research Centre in Frascati (Rome) using a setup made at the ENEA laboratory (see description in Ricci et al., 2016; Caneve et al., 2018; Toffolo et al., 2019). A Thomson DIVA diode pulsed Nd:YAG laser with a UV excitation wavelength of 266 nm was used as radiation source at a repetition rate of 20 Hz with a pulse duration of 8 ns. The spectrometer (Ocean Optics USB 4000) working range was 200–900 nm and appropriate filters were placed at the entrance of the spectrometer in order to avoid the backscattered radiation and the second order of the emissions at lower wavelengths. LIF measurements were performed on untreated samples by scanning point by point and covering a surface of ~1 cm^2. Up to 16 spectra were collected for each sample. Spectrum adjustments such as smoothing and

baseline subtraction were performed using Origin Pro 9 software (Origin Lab Corporation, Northampton, USA). LIF measurements were performed on ~2 mg of powder enamel (≤ 200 μm). Five samples from Lovedale were measured. Both natural and irradiated aliquots (highest dose) were analysed. For comparison, a fossil enamel with low U-content (<10 ppb, powder form) from the Middle Palaeolithic site of Hohle Fels (HF2976) and the modern lamb enamel ('LAM') were measured, the latter both in fragment and powder form, in order to have a reference tooth free of uranium.

References

Asscher, Y., Regev, L., Weiner, S., Boaretto, E., 2011a. Atomic Disorder in Fossil Tooth and Bone Mineral: An FTIR Study Using the Grinding Curve Method. ArcheoSciences 35, 135-141.

Asscher, Y., Weiner, S., Boaretto, E., 2011b. Variations in Atomic Disorder in Biogenic Carbonate Hydroxyapatite Using the Infrared Spectrum Grinding Curve Method. Advanced Functional Materials 21, 3308-3313.

Caneve, L., Spizzichino, V., Antonelli, E., Bertani, L., 2018. Study of ancient egyptians artefatcs by non-destructive laser based techniques, Proceedings of the IEEE International conference on metrology for archaeology and cultural heritage – METROARCHAEO, Cassino (Italy), Cassino (Italy), pp. 374-378.

Farmer, V.C., 1974. The Infrared Spectra of Minerals. Mineralogical Society, London.

Grün, R., 1989. Electron spin resonance (ESR) dating. Quaternary International 1, 65-109.

Grün, R., Schwarcz, H.P., Chadam, J., 1988. ESR dating of tooth enamel: Coupled correction for U-uptake and U-series disequilibrium. International Journal of Radiation Applications and Instrumentation. Part D. Nuclear Tracks and Radiation Measurements 14, 237-241.

Mercier, N., Falguères, C., 2007. Field gamma dose-rate measurement with a NaI(Tl) detector: re-evaluation of the "threshold" technique. Ancient TL 25, 1-4.

Pons-Branchu, E., Douville, E., Roy-Barman, M., Dumont, E., Branchu, P., Thil, F., Frank, N., Bordier, L., Borst, W., 2014. A geochemical perspective on Parisian urban history based on U–Th dating, laminae counting and yttrium and REE concentrations of recent carbonates in underground aqueducts. Quaternary Geochronology 24, 44-53.

Pons-Branchu, E., Sanchidrián, J.L., Fontugne, M., Medina-Alcaide, M.Á., Quiles, A., Thil, F., Valladas Sanchidrián, H., 2020. U-series dating at Nerja cave reveal open system. Questioning the Neanderthal origin of Spanish rock art. Journal of Archaeological Science 117, 105120.

Prescott, J.R., Hutton, J.T., 1988. Cosmic ray and gamma ray dosimetry for TL and ESR. International Journal of Radiation Applications and Instrumentation. Part D. Nuclear Tracks and Radiation Measurements 14, 223-227.

Ricci, G., Caneve, L., Pedron, D., Holesch, N., Zendri, E., 2016. A multi-spectroscopic study for the characterization and definition of production techniques of German ceramic sherds. Microchemical Journal 126, 104-112.

Richard, M., Falguères, C., Pons-Branchu, E., Bahain, J.J., Voinchet, P., Lebon, M., Valladas, H., Dolo, J.M., Puaud, S., Rué, M., Daujeard, C., Moncel, M.H., Raynal, J.P., 2015. Contribution of ESR/U-series dating to the chronology of late Middle Palaeolithic sites in the middle Rhône valley, southeastern France. Quaternary Geochronology 30, 529-534.

Toffolo, M.B., Ricci, G., Caneve, L., Kaplan-Ashiri, I., 2019. Luminescence reveals variations in local structural order of calcium carbonate polymorphs formed by different mechanisms. Scientific Reports 9, 16170.

Weiner, S., Bar-Yosef, O., 1990. States of Preservation of Bones from Prehistoric Sites in the Near East: A Survey. Journal of Archaeological Science 17, 187-196.

Yokoyama, Y., Falgueres, C., Quaegebeur, J.P., 1985. ESR dating of quartz from quaternary sediments: First attempt. Nuclear Tracks and Radiation Measurements (1982) 10, 921-928.

Supplementary figures

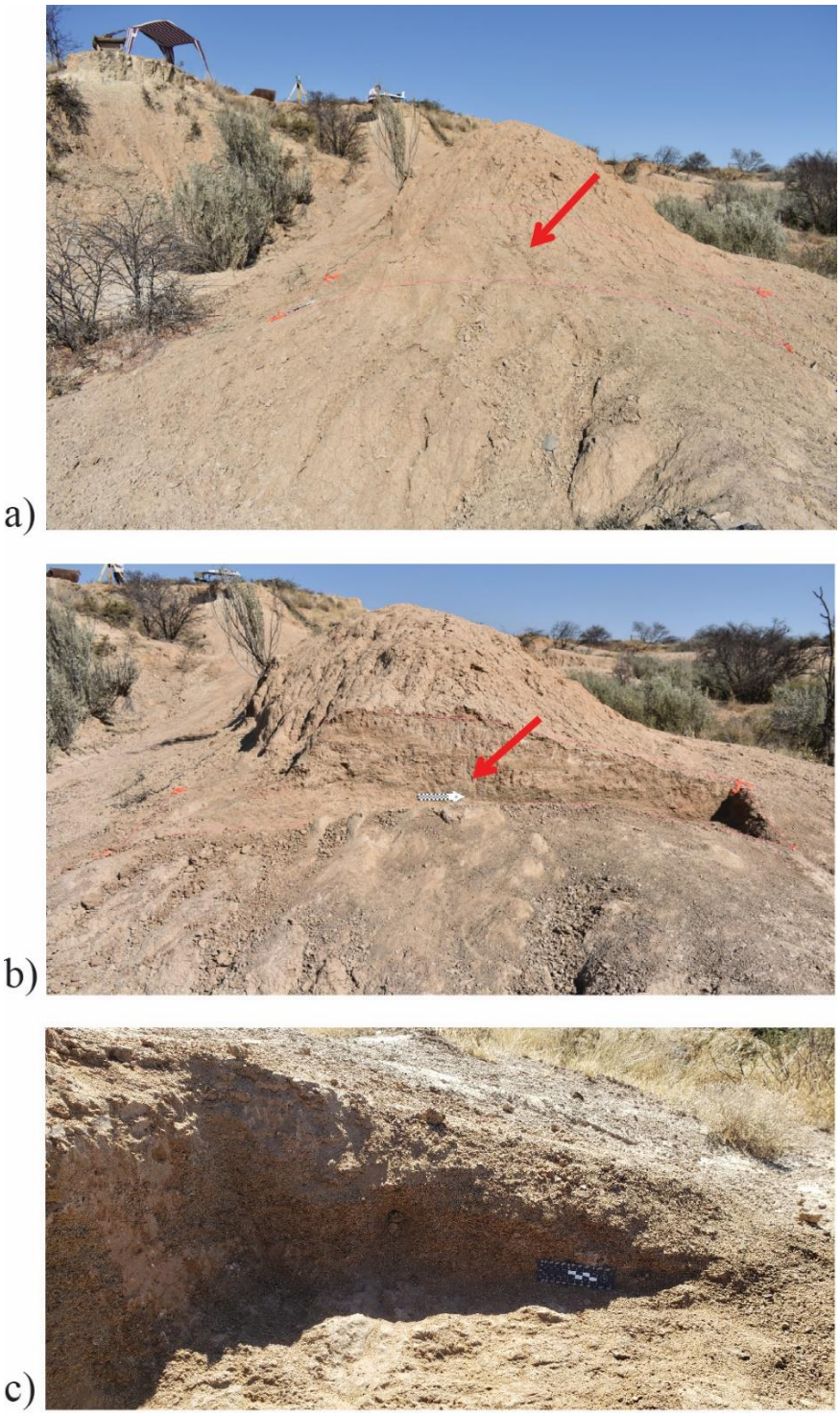

Fig. S1. The gravel layer (Unit 9): a) view before the 2019 excavation season; b) view at the end of the 2019 excavation season (scale bar: 20 cm); c) close-up view (looking north) of the gravel layer at the end of the 2021 excavation season (scale bar: 10 cm).

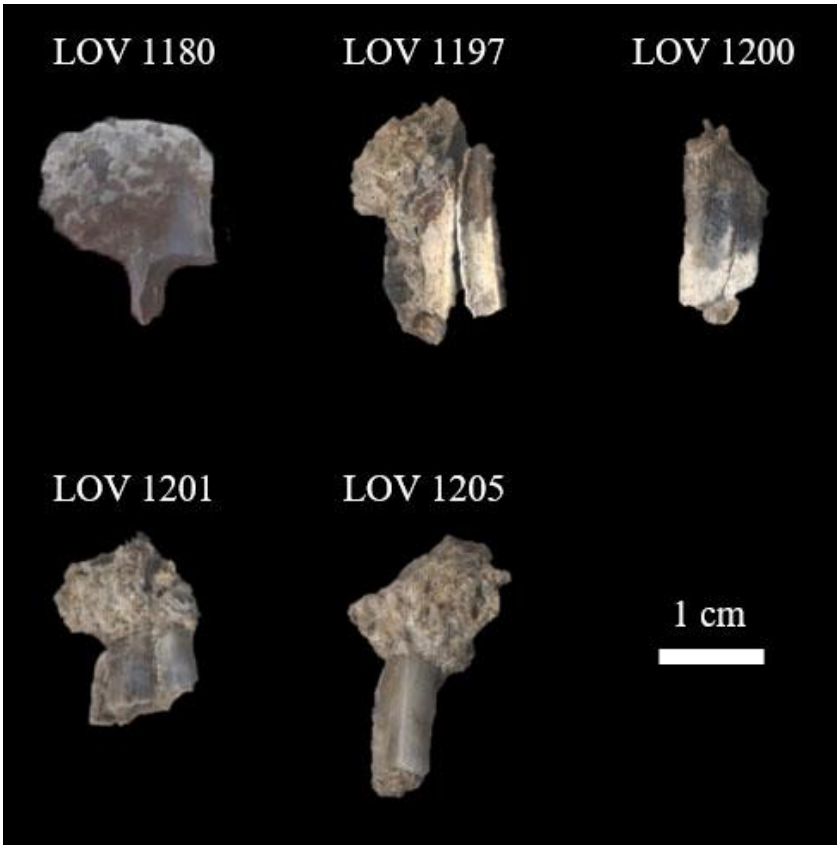

Fig. S2. Photos of the dated samples. Note that LOV 1180 is a tooth fragment.

Fig. S3. Scans of the thin sections obtained from the two intact blocks of sediment taken from the gravel layer. Left: LOV21-2; right: LOV21-1.

Micromorphology (supplementary results):

The coarse gravel facies has a very open structure and is predominantly composed of large (~1-4 mm) grains of shale, quartz, feldspar, and dolerite. Some of the elongated grains appear to have horizontal orientation that creates bands throughout the layer. There is very little fine fraction except for rare pockets of fine silt and clay. This is the microfacies where faunal material was found. The fine gravel microfacies appears at the top of the sequence and is made up of the same components as the coarse gravel but with a somewhat more closed structure, a finer size class of the components, and with a mix of rounded, sub-rounded, and sub-angular grains. There is some fine fraction and a grano-striated b-fabric. This facies also shows an increase in the amount of iron/manganese impregnations, and nodules. The third microfacies is composed primarily of coarse-to-fine sand sized, sub-rounded to sub-angular quartz grains that appear somewhat weathered, fewer silt-sized grains of sub-angular quartz, and rare sub-angular grains of shale. It has a chamber microstructure with a few channels concentrated towards the top of the unit. There is a weakly developed grano-striated b-fabric, as well as stipple-speckled b-fabric in some areas. The silty sand microfacies also shows evidence for iron and manganese with staining and impregnations throughout, as well as coatings in and around void spaces and small nodules (0.5-1 mm). There are also two small lenses of compact sediment that grades from very fine sand sized grains at the bottom to silt sized grains at the top, with rare rounded chambers and cracks. These lenses also have evidence for secondary calcium carbonate formation and striated b-fabric. One of these lenses in the middle portion of the sample profile exhibits areas with a crumb microstructure, and very well-rounded sediment aggregates within void spaces, which are the result of bioturbation during land surface exposure.

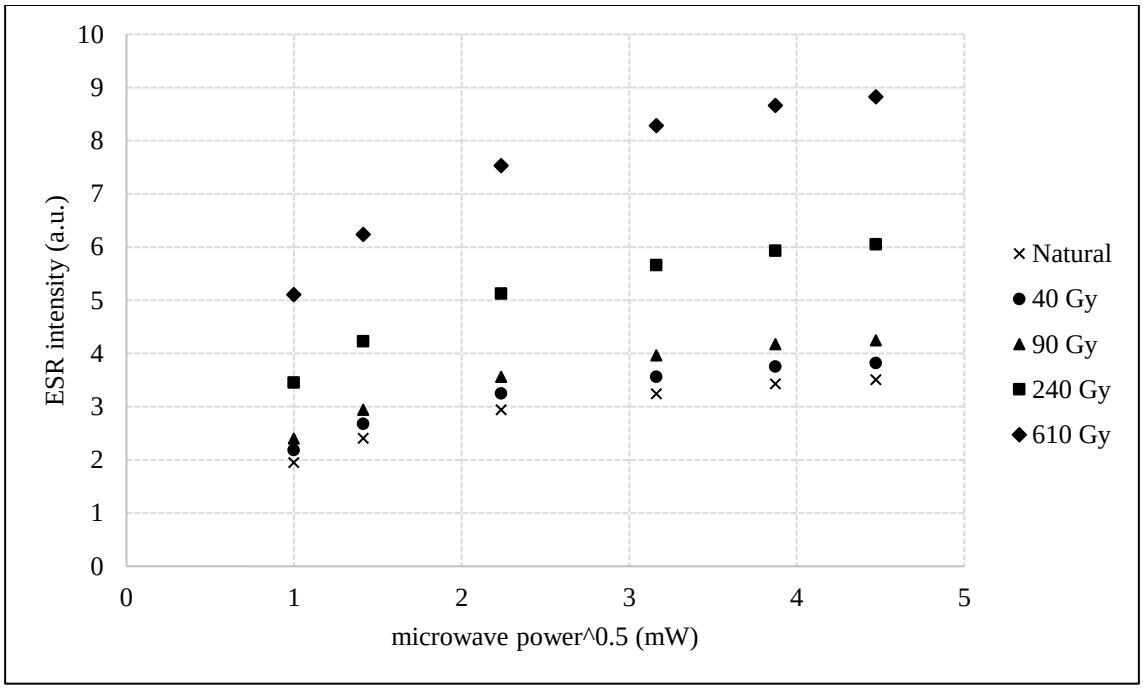

Fig. S4. LOV 1180. Saturation curves obtained for each aliquot as a function of microwave power (1, 2, 5, 10, 15, and 20 mW)

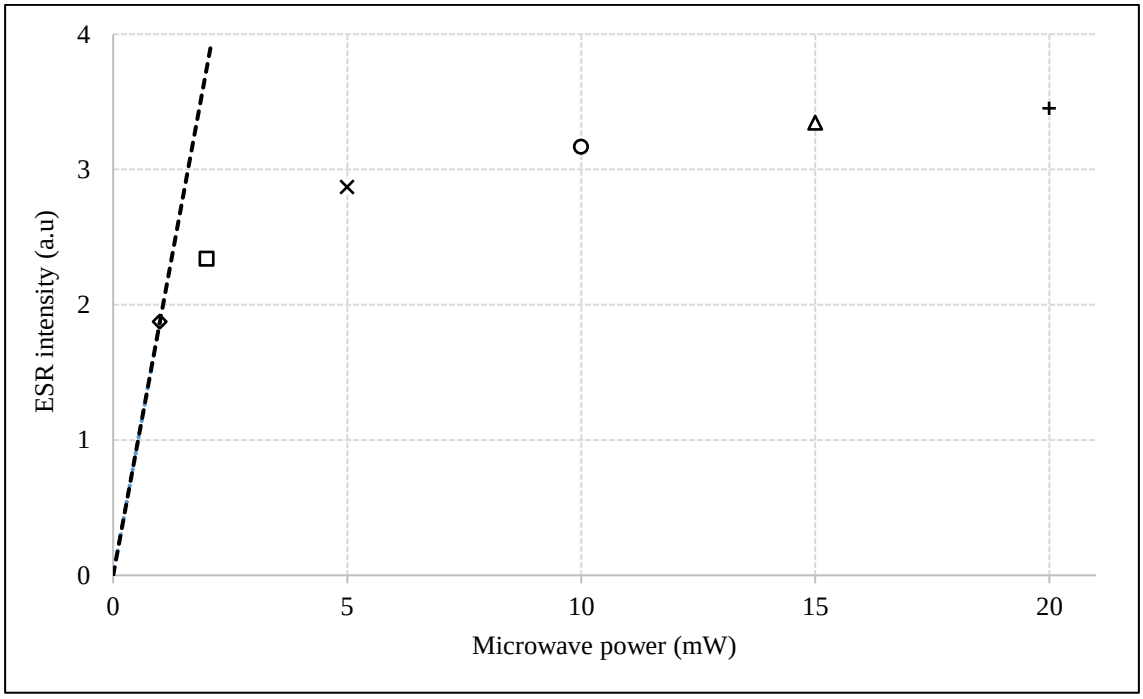

Fig. S5. LOV1180. Saturation curve of the natural aliquot

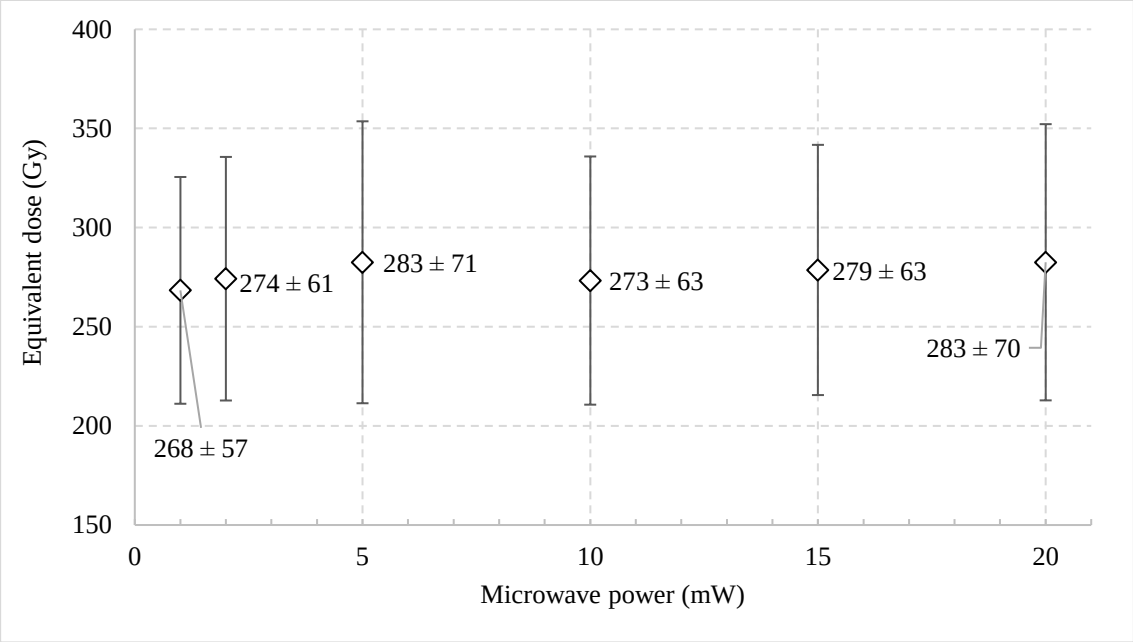

Fig. S6. Equivalent doses obtained as a function of the microwave power used.

a)

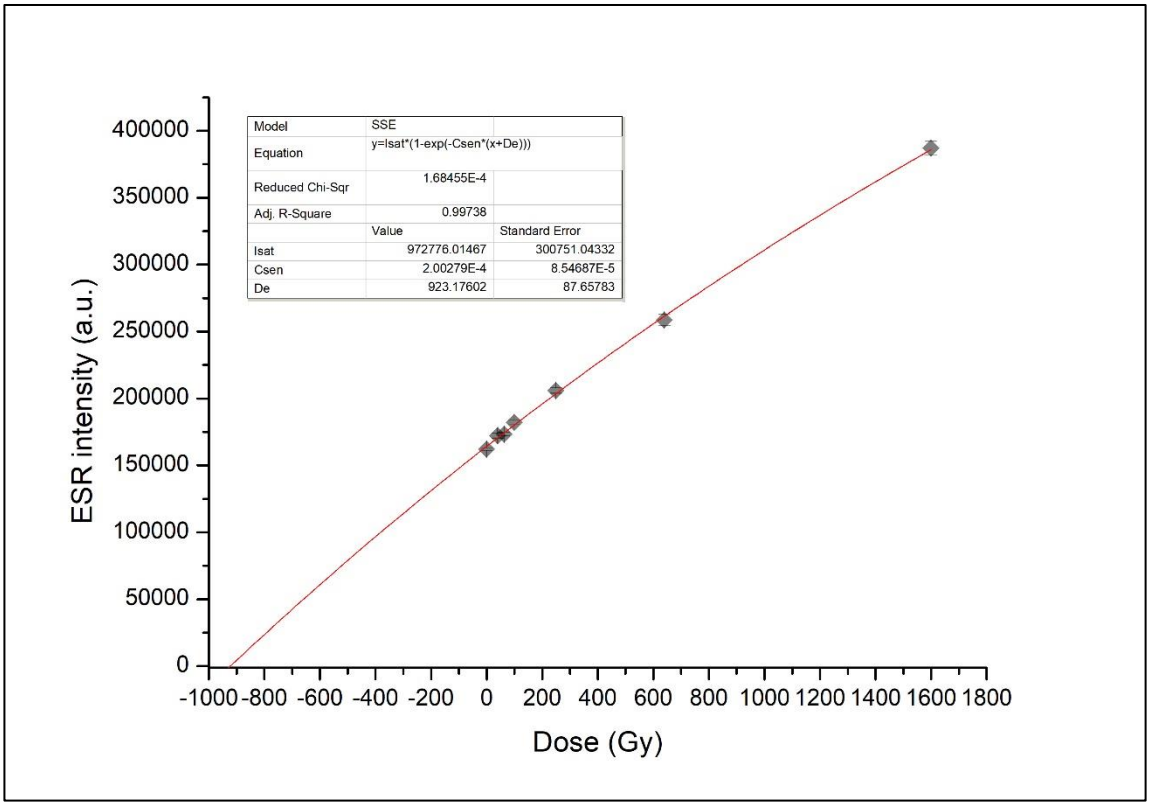

b)

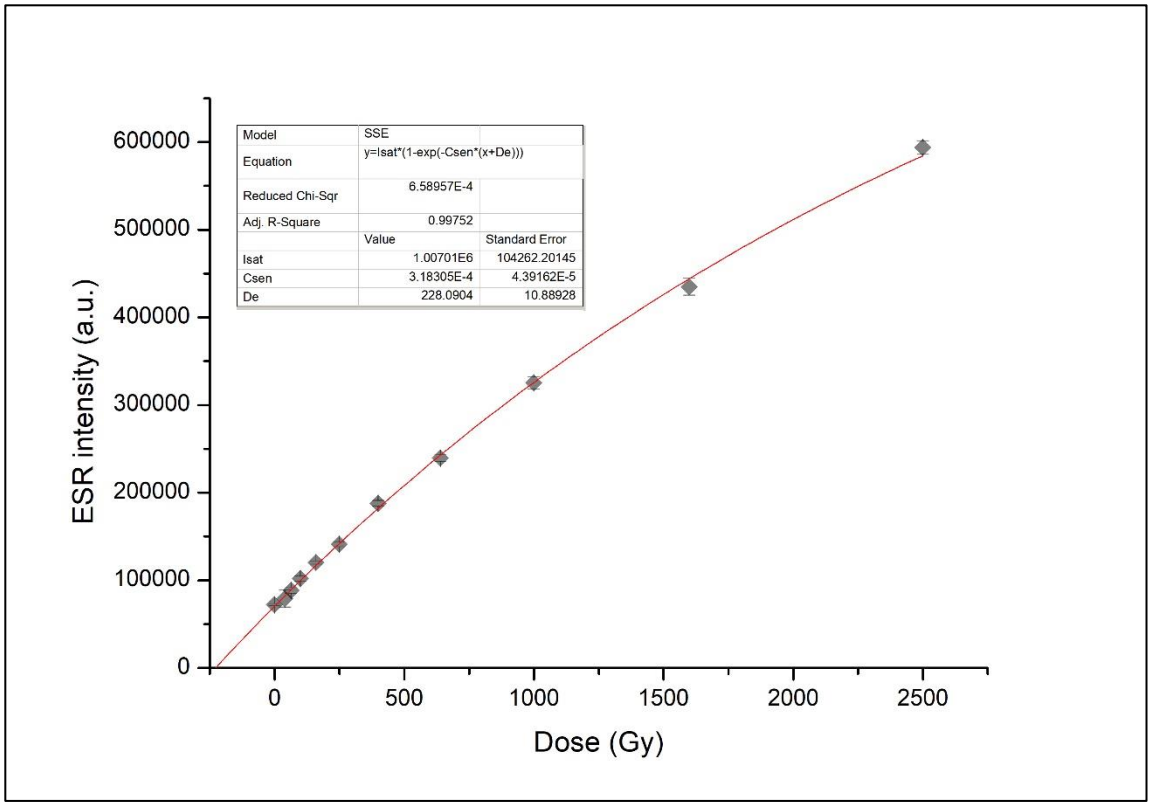

Fig. S7. Dose response curves: a) LOV1200; b) LOV1205.

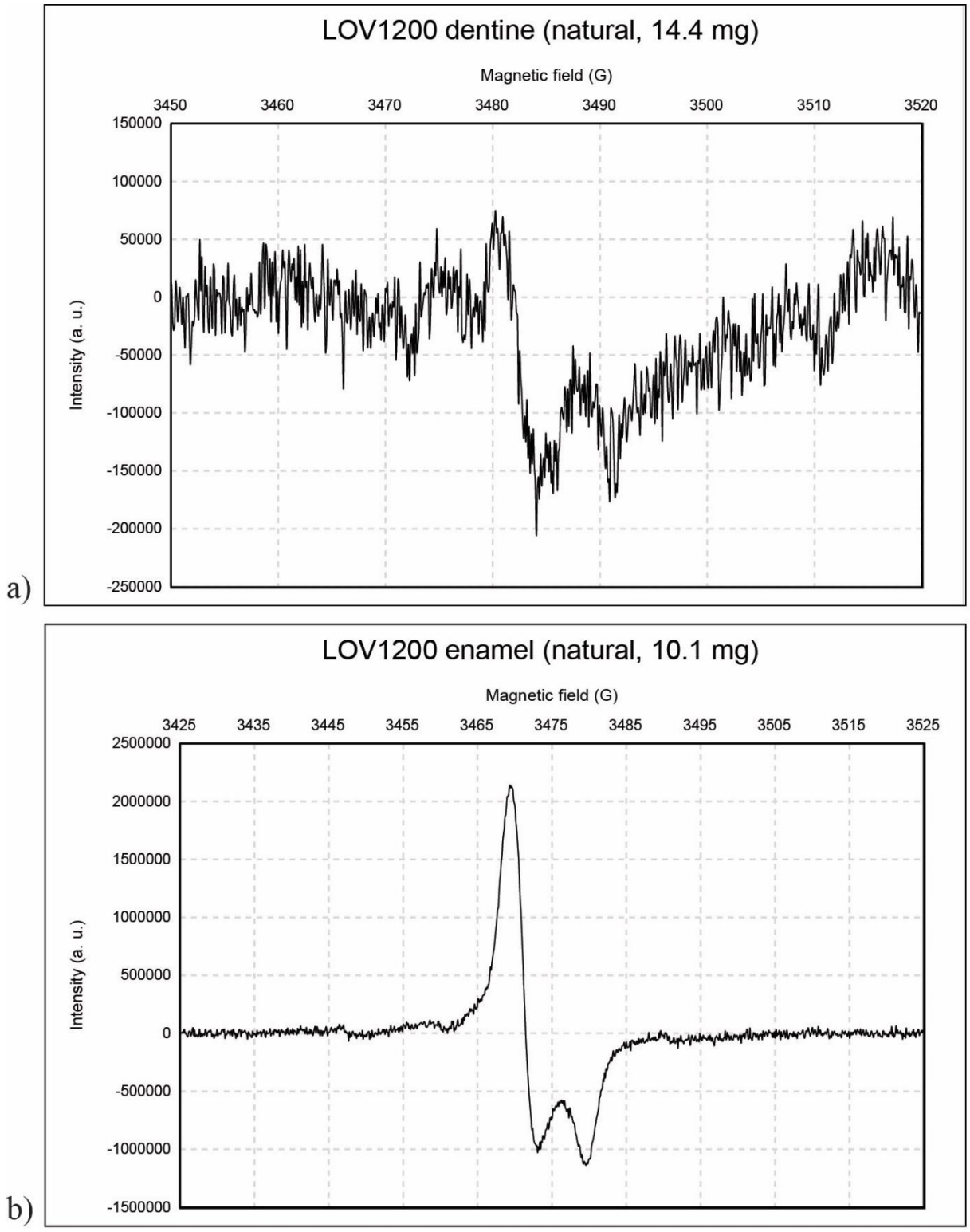

Fig. S8. ESR spectra obtained from LOV1200: dentine (a) and enamel (b) aliquots.

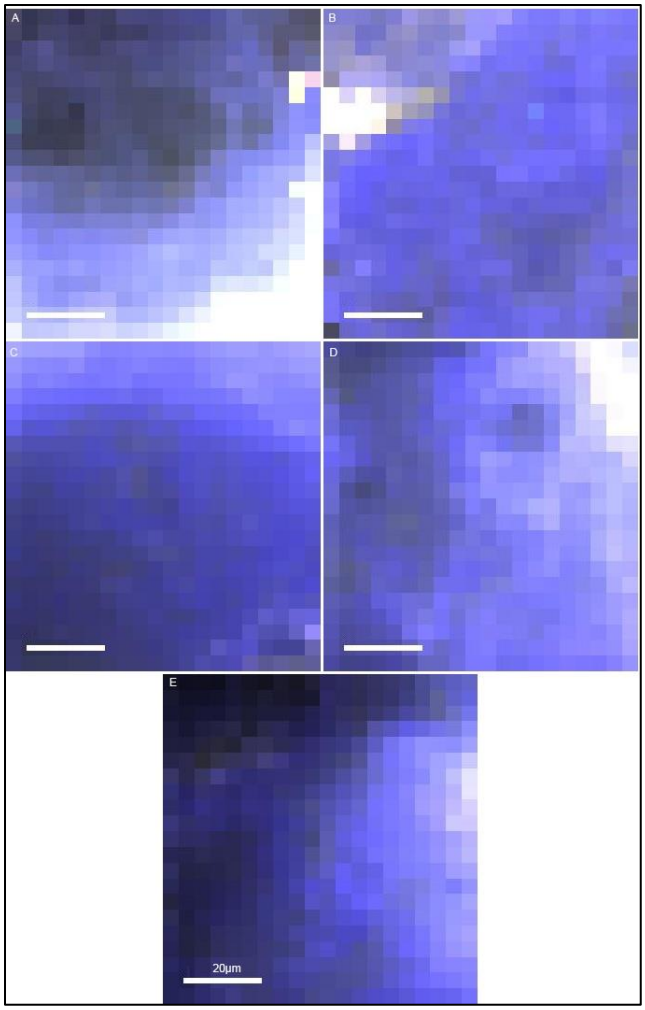

Fig. S9. True colour CL maps of different enamel aliquots of LOV1180: A: 0 Gy; B: 40 Gy; C: 90 Gy; D: 240 Gy; E: 610 Gy. Scale bars: 20 µm.

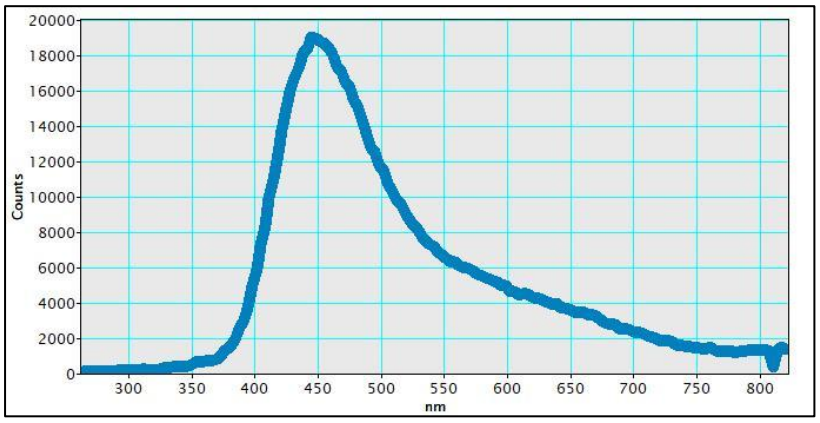

Fig. S10. Representative CL spectrum of Lovedale enamel including a 450 nm emission band. Similar spectra were obtained from all five samples.

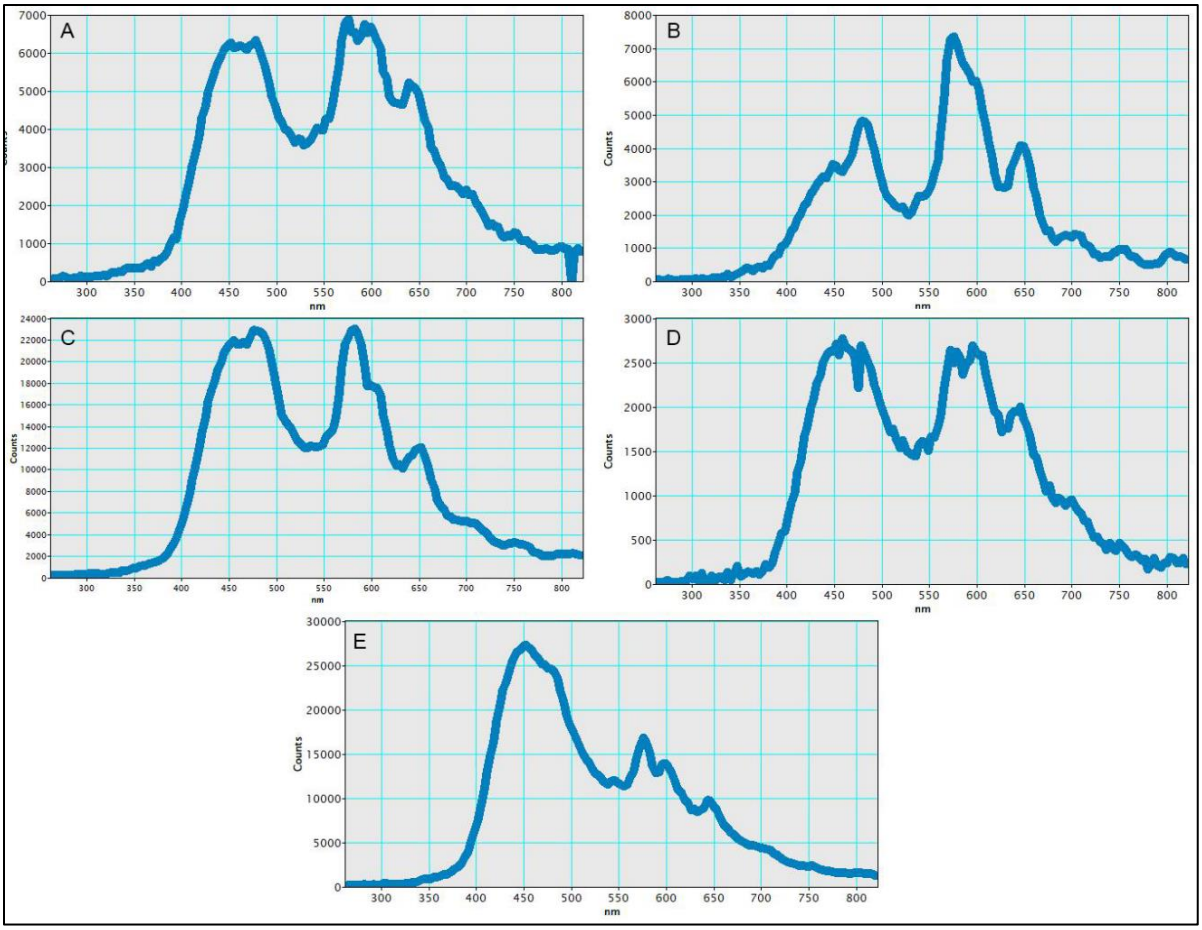

Fig. S11. Representative CL spectra obtained from LOV1180. The sharp peaks can be correlated with Mn^{2+} (600 nm) and REEs such as Dy^{3+} (480 nm, 570 nm), Sm^{3+} (650 nm), Eu^{3+} (620 nm, 700 nm), and Sm^{2+} (720 nm). Each spectrum represents a different aliquot: A) 0 Gy, B) 40 Gy, C) 90 Gy, D) 240 Gy, E) 610 Gy.

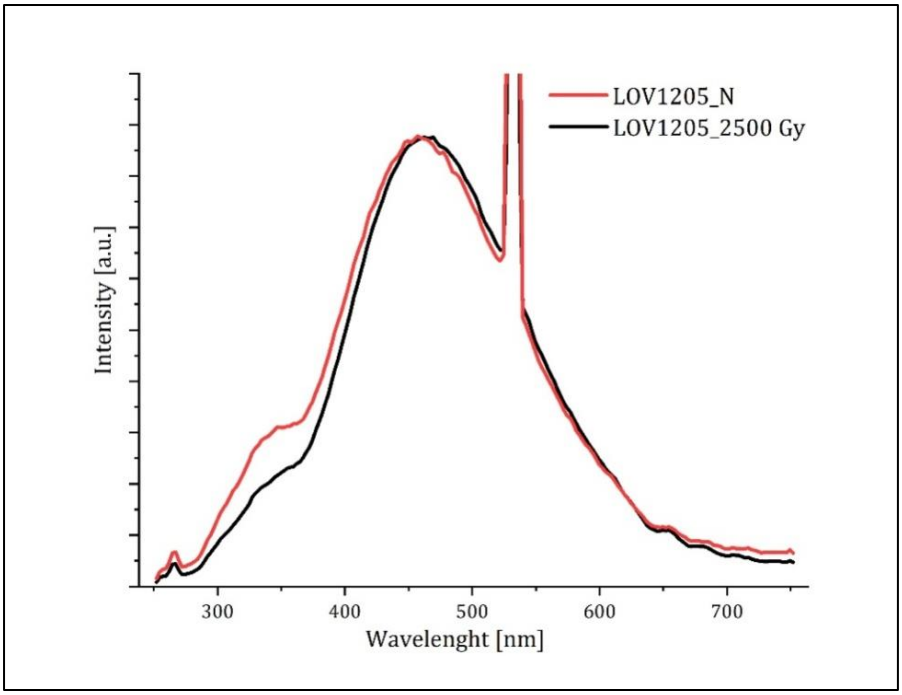

Fig. S12. LIF spectra of the irradiated enamel (2500 Gy) compared to the natural one (N) of LOV1205. The sharp peak at 532 nm is related to the second harmonic of the laser (λ_{exc}=266 nm).

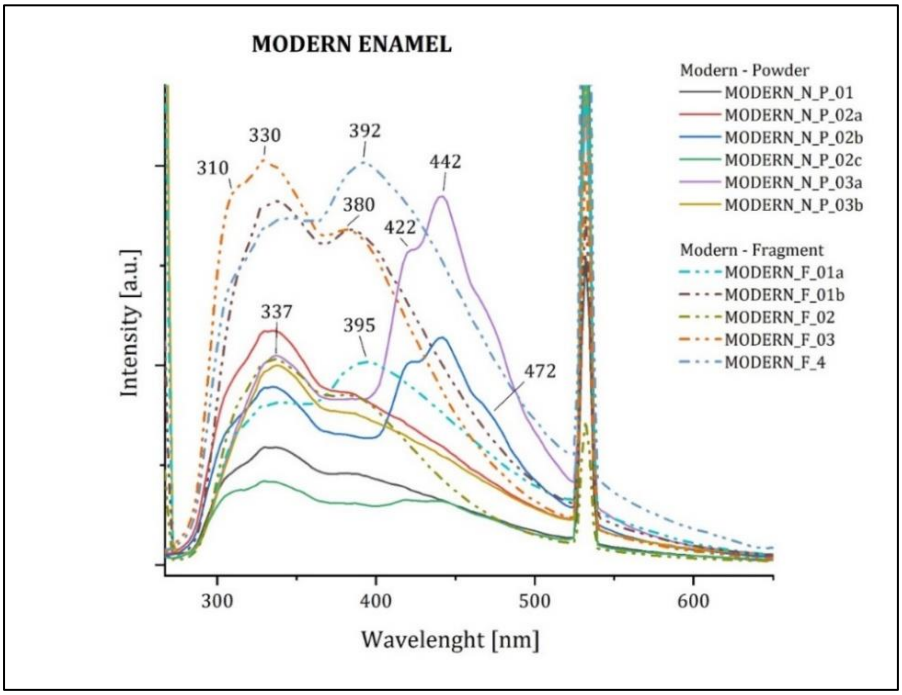

Fig. S13. LIF spectra of modern enamel (lamb) obtained from different points of the same fragment (F) and powder (P).

Tables

Sample	LOV 1180	LOV 1197	LOV 1200	LOV 1201	LOV 1205
Aliquot mass (mg)	9.7-9.9	5.1-5.9	9.3-10.1	10.2-11.0	13.7-14.7
Experimental points	5	7	7	11	11
D_e (Gy)	268 ± 57	449 ± 61	923 ± 88	288 ± 19	228 ± 11
Error D_e (%)	21	14	10	7	5
R^2	0.98933	0.99095	0.99738	0.99507	0.99752
D_{max} (Gy)	610	1600	1600	2500	2500
D_{max}/D_e	2	4	2	9	11

Tab. S1. ESR fitting results (1 σ). The aliquot mass corresponds to minimum and maximum range for all aliquots of a same sample. The number of experimental points includes one natural aliquot + irradiated aliquots. The r^2 is the coefficient of determination and expresses the quality of the fitting of the dose response curve. D_{max} is the maximum irradiation dose.

Sample	Tissue	Lab#	U-series						Enamel thickness (µm)[1]		
			^{238}U (ppm)	^{232}Th (ppb)	(^{234}U/^{238}U)	(^{230}Th/^{234}U)	(^{230}Th/^{232}Th)	^{232}Th/^{238}Th	Initial	Side 1	Side 2
LOV 1180	Enamel	8514	1.72 ± 0.01	37.72 ± 0.32	2.0359 ± 0.0037	0.5487 ± 0.0020	155.5 ± 0.5	0.0219	700	20	20
	Dentine	8515	119.38 ± 1.01	179.68 ± 1.44	2.2162 ± 0.0012	0.6245 ± 0.0005	2834.4 ± 1.9	0.0015			
LOV 1197	Enamel	8574	9.68 ± 0.08	34.99 ± 0.29	2.3092 ± 0.0056	0.6715 ± 0.0020	1315.6 ± 2.4	0.0036	671	87	107
	Dentine	8575	95.44 ± 0.79	55.25 ± 0.49	2.3094 ± 0.0019	0.6771 ± 0.0057	8798.2 ± 73.7	0.0006			
LOV 1200	Enamel	8576	29.56 ± 0.26	97.74 ± 0.88	2.1809 ± 0.0035	0.7579 ± 0.0065	1627.8 ± 13.6	0.0033	510	18	10
	Dentine	8577	105.19 ± 0.92	339.42 ± 2.90	2.0494 ± 0.0022	0.7381 ± 0.0032	1495.8 ± 6.2	0.0032			
LOV 1201	Enamel	8578	2.19 ± 0.02	12.63 ± 0.10	2.2839 ± 0.0020	0.4926 ± 0.0010	599.2 ± 1.0	0.0058	755	23	65
	Dentine	8579	143.07 ± 1.17	111.98 ± 1.00	2.4419 ± 0.0021	0.5390 ± 0.0048	5365.9 ± 47.1	0.0008			
LOV 1205	Enamel	8580	1.90 ± 0.02	69.62 ± 0.57	2.1108 ± 0.0019	0.5659 ± 0.0014	99.9 ± 0.2	0.0366	732	20	20
	Dentine	8581	101.34 ± 0.87	31.00 ± 0.34	2.2600 ± 0.0020	0.6081 ± 0.0064	14325.0 ± 150.3	0.0003			

Tab. S2. U-series results (U content, activity isotopic ratios and ^{232}Th/^{238}Th content ratios) and enamel thickness measurements used for the beta attenuation.

[1]An error of 10% was considered for the measurements of the initial enamel thickness using a digital calliper, and of 10 µm for the removed thickness. Initial=thickness before cleaning the two sides; side 1: dentine: side 2: sediment.

Sample	U (ppm)	Th (ppm)	K (%)
LOV 1197	1.74 ± 0.03	7.59 ± 0.09	1.48 ± 0.03
LOV 1200/1180*	1.94 ± 0.03	7.41 ± 0.08	1.49 ± 0.02
LOV 1201	1.58 ± 0.03	5.81 ± 0.08	1.24 ± 0.02
LOV 1205	3.43 ± 0.04	8.02 ± 0.10	1.54 ± 0.03

Tab. S3. HPGe-gamma spectrometry results: U, Th, and K content from the sediment samples containing the teeth used to derive the beta dose rate.
*Each sediment sample was collected with the tooth it contained except for LOV1180 for which the sediment from the closest tooth was used for dose rate determination.

Sample	IRSF	FWHM (cm^{-1})
SPR-1	3.3	149
SPR-2	3.5	135
SPR-3	3.9	112
LAM-1	3.4	140
LAM-2	3.7	122
LAM-3	3.9	110
LOV1180-1	3.3	148
LOV1180-2	3.7	122
LOV1180-3	4.2	97
LOV1197-1	3.5	142
LOV1197-2	4	117
LOV1197-3	4.5	105
LOV1200-1	3.7	137
LOV1200-2	4.4	114
LOV1200-3	4.7	102
LOV1201-1	3.4	141
LOV1201-2	3.9	114
LOV1201-3	4	109
LOV1205-1	3.2	152
LOV1205-2	3.7	120
LOV1205-3	4	110

Tab. S4. FTIR spectroscopy results. Infrared splitting factor (IRSF) and full width at half maximum (FWHM) calculated for the modern (SPR=springbok; LAM=lamb) and fossil (LOV) samples and used to construct the grinding curves presented in Fig. 4. For a given sample, 1, 2, and 3 refer to the first, second, and third measurements of the same aliquot (increased grinding).

Sample	FWHM (cm^{-1})	Peak location (cm^{-1})
LAM	17.7278	959.8784
SPR	16.3410	960.7192
LOV1180-N	15.5818	960.5648
LOV1197-N	16.0449	960.5676
LOV1200-N	15.6560	961.2171
LOV1201-N	15.9241	960.7689
LOV1205-N	15.4429	960.6267
LOV1180-I	15.5281	960.7410
LOV1197-I	16.0803	960.5278
LOV1200-I	15.6806	961.1380
LOV1201-I	16.1741	960.7346
LOV1205-I	15.4723	960.6699

Tab. S5. Raman micro-spectroscopy results. Full width at half maximum (FWHM) and location of the peak at 961 cm^{-1} measured for the modern (SPR=springbok; LAM=lamb) and fossil (LOV) samples. N refers to the natural aliquots; I to the irradiated ones (highest dose per sample).